Fabrication and properties of mechanically milled alumina/aluminum nanocomposites

Poirier, Dominique; Drew, Robin A. L.; Trudeau, Michel; Gauvin, Robin

Publisher's version / Version de l'éditeur:
https://doi.org/10.1016/j.msea.2010.08.018
Materials science and engineering A, 527, 29-30, pp. 7605-7614, 2010-01-10

Materials Science and Engineering A 527 (2010) 7605–7614

Contents lists available at ScienceDirect

Materials Science and Engineering A

journal homepage: www.elsevier.com/locate/msea

Fabrication and properties of mechanically milled alumina/aluminum nanocomposites

Dominique Poirier[a,*], Robin A.L. Drew[b], Michel L. Trudeau[c], Raynald Gauvin[a]

[a] Mining and Materials Engineering, McGill University, 3610 University Street, Montreal H3A 2B2, Canada
[b] Engineering and Computer Science, Concordia University, 1515 Ste-Catherine Ouest, Montreal H3G 2W1, Canada
[c] Materials Science, Hydro-Quebec Research Institute, 1800 Boul. Lionel-Boulet, Varennes J3X 1S1, Canada

ARTICLE INFO

Article history:
Received 11 March 2010
Received in revised form 2 August 2010
Accepted 9 August 2010

Keywords:
Nanostructured materials
Composites
Mechanical alloying
Mechanical characterisation
Aluminum alloys

ABSTRACT

The reinforcement agglomeration in nanocomposites is a key issue that needs to be solved in order to fully benefit of the gain in strength and ductility associated with the decrease in reinforcement size from microscale to nanoscale. In this study, mechanical milling has been used successfully to disperse nanometric alumina (n-Al_2O_3) in an aluminum matrix. Al_2O_3/Al nanocomposite powders have been produced for various alumina sizes and concentrations. The 10 vol% n-Al_2O_3/Al powders display hardness values near five times higher than pure unmilled Al. A decrease in the Al_2O_3 particle size from 400 to 4 nm has increased the nanocomposite powder hardness by 11%. The microhardness and compression properties of an Al_2O_3/Al nanocomposite compact consolidated by hot pressing were measured. Comparison with modeled values and literature results indicates that the higher experimental yield strength obtained with the addition of n-Al_2O_3 versus micron size Al_2O_3 is due to in situ matrix strengthening.

1. Introduction

Due to their lightweight and high specific strength, particulate reinforced aluminum composites are attractive structural materials for various domains such as automotive and aerospace applications. They also offer moderate fabrication cost, easier manufacturing than continuous fiber composites with reproducible properties and the possibility to use standard or near standard metal working methods [1].

The most common reinforcements for aluminum are silicon carbide (SiC) and alumina (Al_2O_3), due to high availability, low cost and overall good properties [2]. In general, a gain in stiffness of 50% can be obtained with up to 30 vol% of SiC or Al_2O_3 [1]. Strength values reported are more scattered, but an increase of up to 60% can be obtained for the yield and ultimate tensile strength. However, ductility was always found to be reduced with reinforcement addition, as well as toughness [2].

Recently, Al_2O_3/Al nanocomposites have shown great potential with their unique mechanical properties. In one study [3], the tensile strength obtained with 1 vol% n-Al_2O_3 was found to be equivalent to that of the 10 vol% SiC (13 μm)/Al composite produced in the same conditions. If compared with pure Al, 2 vol% n-Al_2O_3 addition improves yield strength of around 66%, hardness of around 50% and tensile strength of around 80%. In another study [4], ultrason casting method was used to dispersed 2 wt% Al_2O_3 (10 nm) in aluminum. Compared with pure Al casted following the same method, composite hardness was increased by 92% and the yield strength by 56%. Research studies on other nanocomposites have shown an increase in strength combined with an improvement of ductility [5–7].

However, the processing of composites with nanoreinforcement is still an issue. In the two papers cited above involving Al_2O_3/Al [3,4], it has not been possible to obtain the homogeneous distribution needed for optimized properties.

High energy mechanical milling was found to eliminate clustering issue for several nanocomposites [8–11]. It leads to uniform distribution of the reinforcements as well as inducing a significant grain size reduction and lattice strains, also beneficial to strength properties. Furthermore, the reinforcing phase helps to maintain the submicron grain size obtained from milling by pinning grain boundaries during subsequent processing, such as extrusion. However, only one work [8] was found on the possibility of using high energy mechanical milling for dispersion of nanoscale alumina particles in aluminum. The resulting strengthening of the materials was not evaluated.

This paper first intends to evaluate mechanical milling as a possible dispersion method for Al_2O_3/Al nanocomposites. The extent

* Corresponding author. Permanent address: Industrial Materials Institute, 75 Mortagne, Boucherville, Canada. Tel.: +1 450 641 5294; fax: +1 450 641 5105.
E-mail addresses: Dominique.Poirier@mail.mcgill.ca (D. Poirier), rdrew@encs.concordia.ca (R.A.L. Drew), trudeau.michel@ireq.ca (M.L. Trudeau), Raynald.Gauvin@mcgill.ca (R. Gauvin).

0921-5093/$ – see front matter © 2010 Elsevier B.V. All rights reserved.
doi:10.1016/j.msea.2010.08.018

of Al_2O_3 dispersion is evaluated, together with the effect of milling on Al matrix microstructure. The effect of Al_2O_3 size on composite strengthening is also studied through comparison of the measurements obtained in this study with previous experimental results and with modeling.

2. Experimental procedures

Three different sizes of Al_2O_3 powder were tested. Spherical Al_2O_3 of 4 nm nominal size was bought from Aldrich. From observations with a FE-SEM Hitachi S-4700, the average particle size was measured to be 25 nm. Spherical Al_2O_3 of 80 nm average particle size was produced by combustion synthesis [12]. Finally, calcined equiaxed Al_2O_3 was bought from Whittaker, Clark and Daniels (now MPSI) with a nominal particle size of 400 nm but a measured average particle size closer to 310 nm. The size distributions of the three Al_2O_3 sizes measured by FE-SEM are shown in Fig. 1. Spherical Al powder of −325 mesh, 99.5% purity was also used to produce the composite powders. Fig. 2 shows the various Al_2O_3 powder used.

Fig. 3 shows that all Al_2O_3 powders used have the tendency to form agglomerates of similar size of around 50 μm. However, the 400 nm Al_2O_3 has around half of its particles dispersed and the agglomerates present seemed more loosely packed.

As a reference test, Al powder was first milled alone for 5 h under argon atmosphere in a high energy Spex 8000 mill with a rpm of 1200. 2 wt% stearic acid was added as a process control agent to avoid excessive sticking and agglomeration of the aluminum [13]. Tungsten carbide balls (11 mm) and container with a 10:1 ball-to-powder ratio were used. Mixtures of Al_2O_3/Al with concentration varying from 1 to 10 vol% were then milled for each type of alumina powder using the same procedures. The milled Al mixture with no Al_2O_3 addition and the 10 vol% Al_2O_3 mixtures were cold press at 500 MPa and then hot pressed in an uniaxial press at a pressure of 350 MPa and at a temperature of 450 °C for 1 h under vacuum in order to obtain sintered cylinders of 2.5 cm in diameter and around 0.6 cm height.

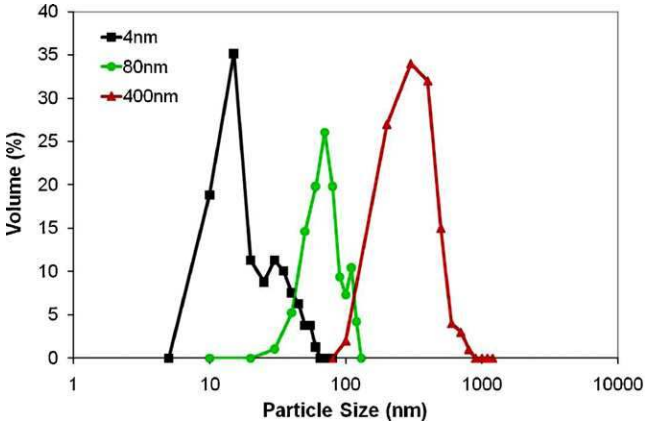

Fig. 1. Size distributions for the different Al_2O_3 powders used.

Dispersion of the Al_2O_3 within the Al powders was studied using a FE-SEM Hitachi S-4700. A CM200 TEM from Philips was used to have a closer look at the second phase and to measure the grain size of the powders. For each sample, the Feret diameter of at least 30 grains was measured. Also, a TEM thin film of the hot pressed 10 vol% Al_2O_3 mixture (4 nm) compact was prepared from grinding followed by electropolishing in a solution of 25% HNO_3 in methanol at −40 °C. From the hot pressed 10 vol% Al_2O_3 mixture (80 nm) compact, a FIB specimen was produced using a NB5000 NanoDue't from Hitachi. This last specimen was observed in a Hitachi HD-2700 dedicated STEM in bright field (BF) and Z-contrast (ZC) mode.

XRD characterization of the powders was performed with a Rigaku Rotaflex Ru-200B type using Cu $K\alpha_1$ radiation at 4.8 kW. The Williamson and Hall method [14] was used to relate the broaden-

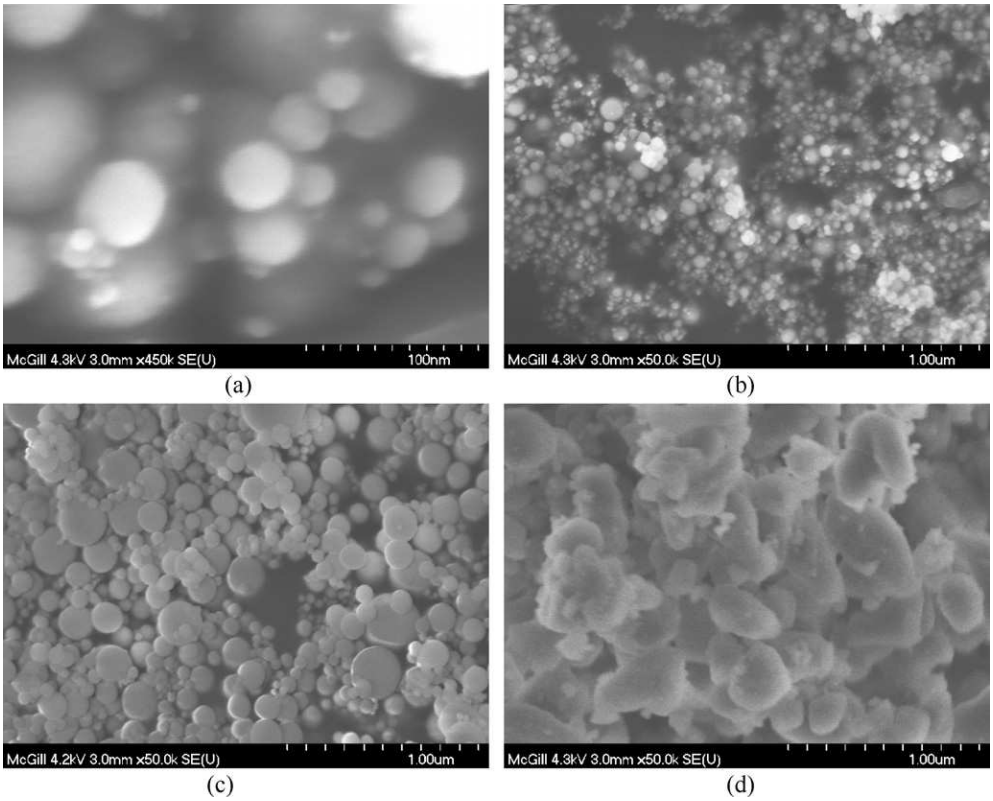

Fig. 2. FE-SEM micrographs of the three Al_2O_3 powders used: (a and b) 4 nm, (c) 80 nm, and (d) 400 nm.

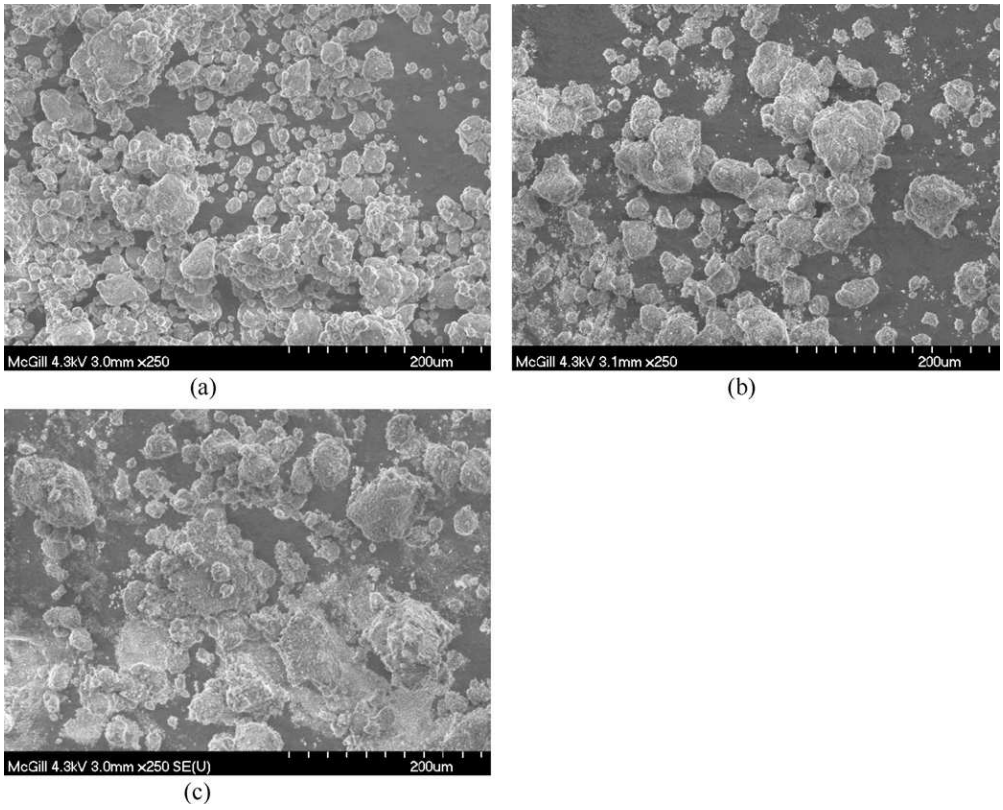

Fig. 3. SEM micrographs of the three Al_2O_3 powders showing initial agglomeration: (a) 4 nm, (b) 80 nm, and (c) 400 nm.

ing of the X-ray peak (B) to the crystallite size (L) and the lattice strain (η), in the form:

$$B\ \cos\theta = \frac{k_s\lambda}{L} + \eta \sin\theta \quad (1)$$

k_s being the Scherrer's constant. The Scherrer's constant, also identified as a geometrical factor, was fixed at 1. The total broadening (B_T) was found by dividing the peak area by its height. The broadening due to the instrument (B_I), found with a reference annealed Al sample, was removed from each peak using the geometrical mean defined as [14]:

$$B = ((B_T - B_I) * (B_T^2 - B_I^2)^{1/2})^{1/2} \quad (2)$$

For each milled mixture, a plot of $B^*\cos\theta$ as a function of $\sin\theta$ was drawn to find the lattice strain and crystallite size.

Microhardness of the powders as well as of the compacts was evaluated using a Vicker microhardness indentor with a load of 50 g and a dwell time of 15 s. It was ensured that this load was low enough to obtain indents much smaller than the particles of powder probed. Each time, the indents were surrounded by at least three times their size of the material being tested. Rectangular samples of 5 mm × 5 mm × 7.5 ± 0.3 mm were machined from the compacts and tested in compression at a rate of $5 \times 10^{-4}\ s^{-1}$ with a MTS Sintech30/G machine.

3. Results and discussion

After milling of the Al_2O_3 powder with the aluminum for 5 h, equiaxed Al powders are obtained where Al_2O_3 particles seem to be well distributed. Fig. 4 shows the 80 nm Al_2O_3 particles distributed at the surface of the Al powder. A low amount is observed

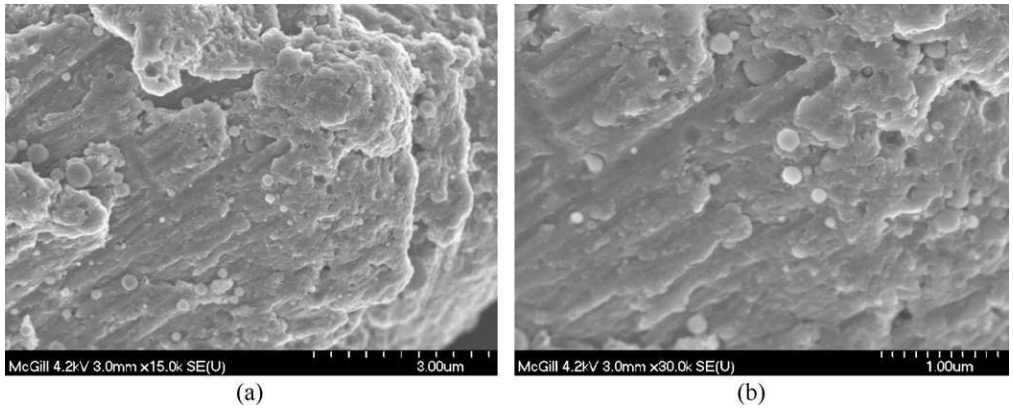

Fig. 4. (a) Low and (b) high magnification of the 5 h milled Al powder with 10 vol% Al_2O_3, 80 nm.

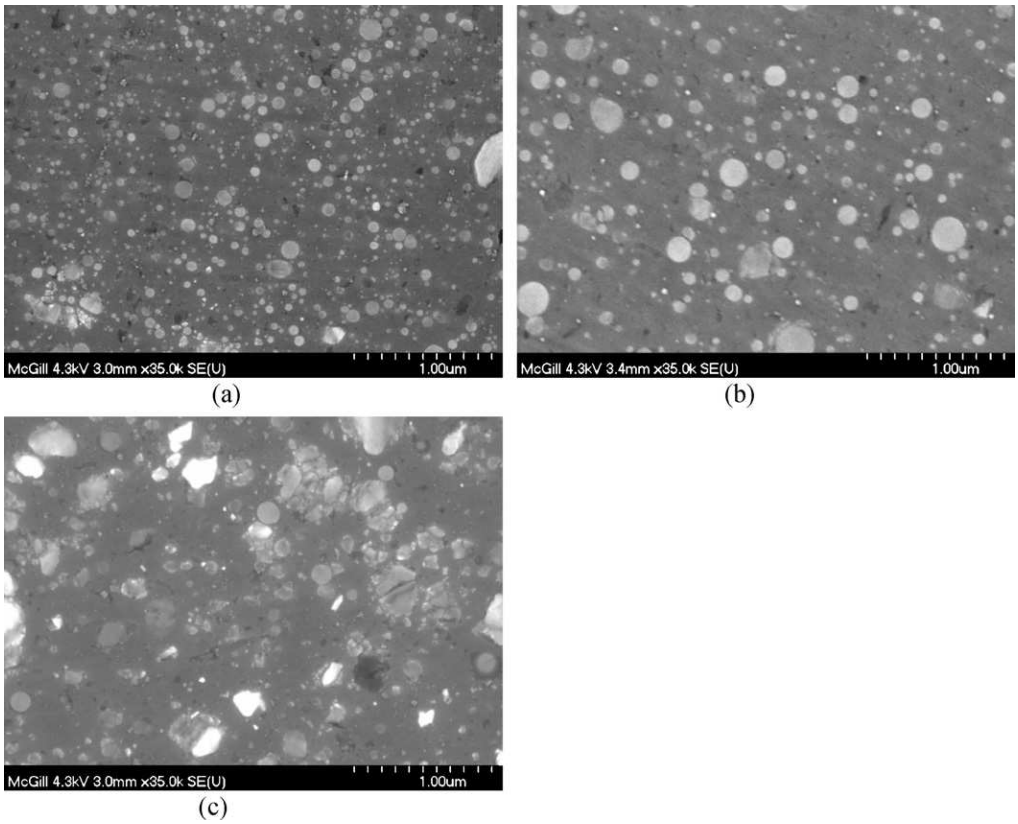

Fig. 5. Al_2O_3 particles within the Al_2O_3/Al hot pressed compacts: (a) 4 nm, (b) 80 nm, and (c) 400 nm.

because the remaining Al_2O_3 is now embedded in the Al particles.

The dispersion of the Al_2O_3 within the Al was observed in the hot pressed compacts for the three Al_2O_3 size. From the SEM micrographs shown in Fig. 5, the 4 and 80 nm Al_2O_3 powders appear very well dispersed in Al. Their spherical shape and their size have been preserved during milling. Closer observation of Al_2O_3 dispersion in the hot pressed 10 vol% Al_2O_3 (4 nm) compact through TEM (Fig. 6) revealed few agglomerates with size of around 1 μm.

The 400 nm Al_2O_3 compact displays minimal agglomeration on the SEM micrograph (Fig. 5c), maybe due to the initial angular shape of the Al_2O_3 powder. Also, the Al_2O_3 was broken during milling and the average Al_2O_3 size has decreased by half from 310 to 130 nm. This significantly decreases the difference in size with the 80 and 400 nm nominal Al_2O_3 powders.

The crystallite size (L) and the lattice strain (η) calculated from the Williamson and Hall method are presented for each milled mixture in Tables 1 and 2. The grain sizes of the mechanically milled Al, the 10 vol% Al_2O_3 (4 nm) mixture and the 10 vol% Al_2O_3 (400 nm) mixture were also measured using TEM. The average grain sizes obtained were of 60, 50 and 160 nm respectively. TEM values are consistently about half the values obtained with XRD measurements. Part of the explanation for this discrepancy is that XRD method leads to volume-weighted mean of grain size distribution. Bigger grains contribute more to the weighted mean than the smaller grains. On the other hand, the arithmetic mean is usually taken to average the grain sizes from TEM measurements and this

Table 1
Al crystallite size of the milled powders according to Al_2O_3 content and size.

Conc.	Al_2O_3 size		
	4 nm	80 nm	400 nm
0%	110 nm		
1%	120 nm	110 nm	140 nm
2%	100 nm	90 nm	120 nm
10%	90 nm	180 nm	310 nm

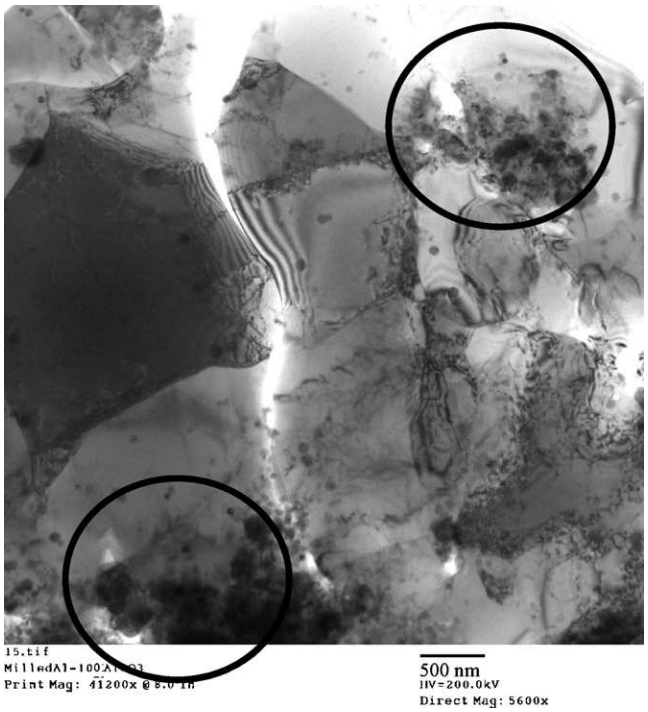

Fig. 6. TEM micrograph of the 10 vol% Al_2O_3 (4 nm) thin film showing few Al_2O_3 agglomerates.

Table 2
Al lattice strain of the milled powders according to Al_2O_3 content and size.

Conc.	Al_2O_3 size		
	4 nm	80 nm	400 nm
0%	0.0054		
1%	0.0050	0.0062	0.0062
2%	0.0048	0.0050	0.0058
10%	0.0050	0.0076	0.0080

value is typically smaller. Those looking for further details regarding grain size extraction from XRD patterns and how the calculated means can be compared to TEM measurements are referred to [15]. In our specific case, if volume-weighted means are calculated from TEM grain size measurements, then 66, 62 and 270 nm are obtained for the mechanically milled Al, the 10 vol% Al_2O_3 (4 nm) mixture and the 10 vol% Al_2O_3 (400 nm) mixture respectively. The effect is especially remarkable for the 10 vol% Al_2O_3 (400 nm) mixture, where the difference between TEM and XRD measurements is significantly reduced. However, other explanations are needed for the remaining gap. Inaccuracies are introduced by the numerous assumptions of the Williamson and Hall method. Among others, the annealed Al powder grains are suspected to be in the order of 500 nm. In that case, the reference peak broadening would be larger than the instrumental broadening alone, and would bias the results. From our calculations using Eqs. (1) and (2), this can account for a variation of about 10 nm. Also, as the size of only 30 grains per mixture was measured under TEM, inaccuracies certainly arise from sampling statistics. Finally, TEM grain size measurement on powders can be bias because it is limited to the electron transparent areas on the particle sides. It can be speculated that the impacts occurring during milling create more deformation on the particle surface than in the middle. As such, the grains could be bigger in the center of the particles.

From XRD grain size measurements, it is seen that a grain size of around 100 nm is typically obtained for the milled mixtures, with or without Al_2O_3 additions. However, the grain sizes of the 10 vol% Al_2O_3 (80 and 400 nm) mixtures are significantly higher, especially for the 400 nm Al_2O_3 size. Furthermore, the lattice strains calculated for those two mixtures are higher than the average lattice strains observed in the other cases. This indicates that the final break down of the Al crystals has not occurred for those two mixtures. It seems the mechanical milling process has been slowed down, as well as the resulting grain refinement. In literature, the addition of a second phase during mechanical milling is rather associated to an acceleration of the milling process. The hard second phase particles act as extra miniballs that accelerate the milling process. Also, the local deformation of the matrix in the vicinity of the reinforcement particles is increased, accelerating the work hardening of the matrix, and thus, the extent of grain refinement [8]. Two hypotheses are suggested here to explain this discrepancy. There could be a critical size and concentration for which the second phase will form a type of protective skeleton. This skeleton would slow down the milling process by absorbing a fraction of the energy during collisions with the balls. Also, it has been shown that the 400 nm Al_2O_3 was broken down during milling. This would absorb another fraction of the impact energy. While no clear evidence are available to validate those hypotheses, it is worth mentioning that a similar behavior was observed during the equal channel angular pressing (ECAP) of an Al_2O_3/Al composite with similar Al_2O_3 concentration and size (10 vol%, 270 nm) [16]. After deformation, the grain size obtained with the composite was higher than the grain size obtained with pure Al in the same conditions. The effect was attributed to the presence of Al_2O_3.

Table 3 presents the microhardness of the milled mixtures and Table 4 those of the hot-pressed compacts. It is seen that milling of

Table 3
Microhardness of the milled powders according to Al_2O_3 content and size.

Conc.	Size		
	4 nm	80 nm	400 nm
0% (initial)	30 ± 7		
0% (milled)	142 ± 5		
1%	147 ± 5	147 ± 8	140 ± 5
2%	151 ± 4	155 ± 5	153 ± 8
5%	163 ± 6	156 ± 4	154 ± 5
10%	166 ± 4	152 ± 4	150 ± 7

Table 4
Microhardness of the hot pressed compacts with 10 vol% Al_2O_3.

Size	Milled Al	4 nm	80 nm	400 nm
Rel density (%)	97	95	95	94
Hardness	164 ± 5	183 ± 9	177 ± 5	173 ± 9

the Al, even without Al_2O_3 addition, increases the hardness around five times from 30 to 142. Deformation occurring during milling leads to cold working and grain refinement [17]. Also, various contaminants coming from the addition of the process control agent, wearing of the balls and vial, the initial oxide layers at the surface of the Al particles or the extra oxidation occurring during the milling process, are embedded in the Al powder where they can form either a solid solution or dispersoids [18]. All those phenomena contribute to the strengthening observed after milling.

From Table 3 and Fig. 7, it is seen that the 80 and 400 nm Al_2O_3 powders have a similar strengthening behavior. This is due to the breaking of the 400 nm Al_2O_3 particles during milling that had created a size distribution close to the 80 nm alumina powder. For all Al_2O_3 particle sizes, an increase in hardness is obtained when 5 vol% Al_2O_3 is added, and then hardness gain level off with further Al_2O_3 addition. This concentration threshold was also observed elsewhere [3]. It was attributed to three factors: a saturation of the grain boundary with nano-particulate, stopping further grain-refinement, a grain boundary embrittlement, due to nano-particle aggregates, and a reduction in effective nano-particle content due to aggregates. In this study, Al_2O_3 was evenly distributed within the grains: nano-particle segregation at grain boundaries has not been observed (Fig. 8). However, the small Al_2O_3 agglomerates presented previously in Fig. 6 could reduce the effective nano-particle content.

The highest powder hardness value of 166 is reached with the 10 vol% Al_2O_3 (4 nm). This corresponds to an improvement of 15%

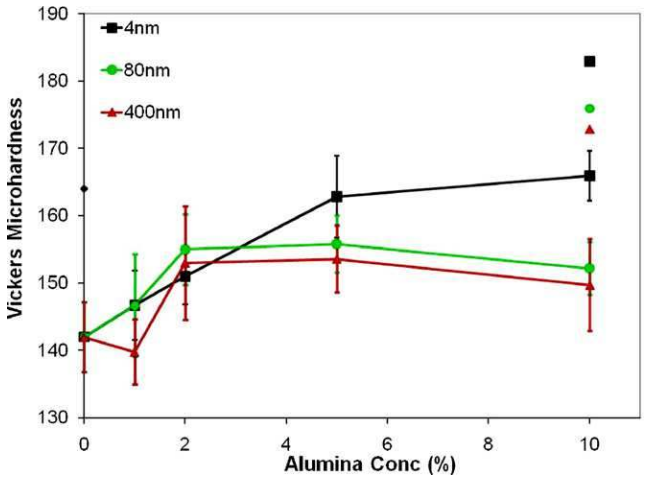

Fig. 7. Microhardness of the milled powders according to Al_2O_3 content and size. The individual dots indicate the hardness of the hot pressed counterparts.

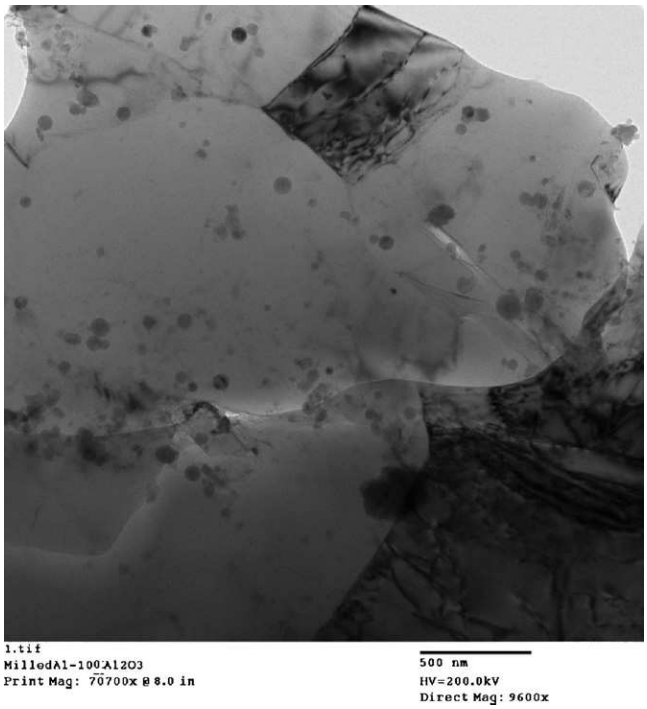

Fig. 8. TEM micrograph of the 10 vol% Al_2O_3 (4 nm) thin film showing uniform dispersion of Al_2O_3 particles within grains.

compared to the milled Al. At this concentration, the hardness difference between the 4 nm Al_2O_3 and the other Al_2O_3 sizes is accentuated. This trend is probably due to the difference in Al grain sizes for the different Al_2O_3 sizes. The 10 vol% Al_2O_3 (4 nm) mixture contains much smaller grains than the 10 vol% Al_2O_3 (80 and 400 nm).

The hardness of the hot pressed mixtures was in all cases increased by around 20 compared with the powder mixtures. This increase in hardness is associated to the heat treatment occurring during hot pressing where the elements present in solid solution after milling precipitate. Among others, aluminum carbide precipitates are obtained, as seen on the XRD pattern below (Fig. 9) of the milled Al before and after a heat treatment at 450 °C for 1 h simulating the hot pressing process. The carbon atoms needed to form the carbides come from the decomposition of the stearic acid added as a process control agent. A similar study involving milled Al powder has also shown an increase in powder nanohardness after heat treatment at the same temperature (450 °C) [19].

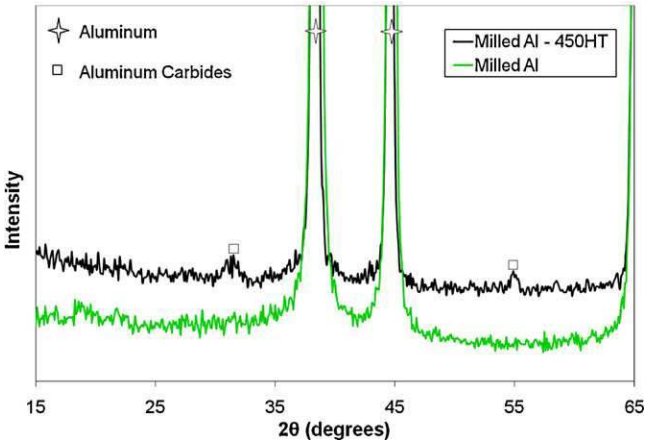

Fig. 9. XRD pattern of the milled aluminum, before and after heat treatment at 450 °C.

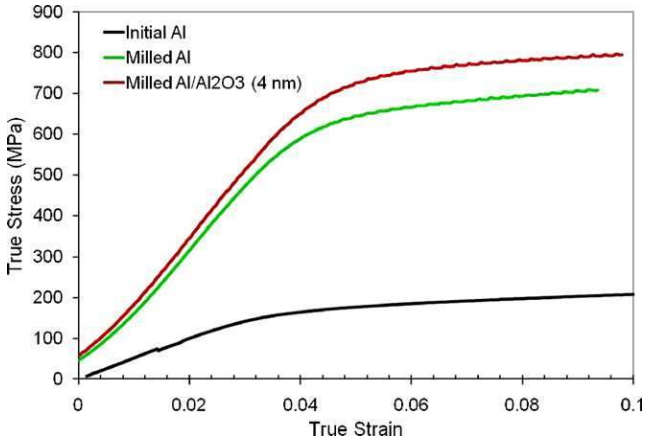

Fig. 10. True stress/true strain curves resulting from the compression tests.

During hot pressing, the milled mixtures are subjected to grain growth due to the applied heat. Due to the limited electron transparent area of the 10 vol% Al_2O_3 (4 nm) thin film, it was not possible to observe enough grains to obtain an average size value. The sizes of the few grains seen range between 0.5 and 1 μm. This is a grain growth significantly higher than what is typically obtained from the consolidation of nanocrystalline Al produced by mechanical milling [17]. In previous studies, the thermal stability of the grains was explained by the pinning forces of the impurities and dispersoids formed during milling [20]. According to this theory, the addition of n-Al_2O_3 should further prevent grain growth. One explanation for the excessive grain growth would be the application of a pressure together with a high temperature during hot pressing that would accelerate grain coarsening [17].

Fig. 10 and Table 5 present the results obtained from the compression tests of the hot pressed compacts. Error bars are not indicated on the graph for the sake of clarity, but the maximum standard deviation for all type of materials was of 15 MPa. Similarly to microhardness results, a higher gain in strength is obtained from milling. Compared with the initial Al, the yield strength and the compression strength of milled Al is increased of about 450 MPa. Al_2O_3 addition further strengthens the aluminum by about 80 MPa to reach a yield stress and compression strength of 661 and 723 MPa respectively.

In order to have a better understanding of the strengthening mechanisms involved with Al_2O_3 addition, the gain in yield strength predicted from common models used in particulate composite strengthening: load transfer, thermal mismatch and Orowan looping, were calculated for an alumina size of 25 nm, which is the actual size of the nominal 4 nm Al_2O_3. The load transfer model, also known as the continuum approach, is based on the load sharing between the matrix and the reinforcement. On the other hand, thermal mismatch and Orowan looping are two in situ strengthening models where the matrix properties are modified by the reinforcement.

The rule of mixture was used for the load transfer model [21]:

$$\sigma_c = V_p\sigma_p + (1 - V_p)\sigma_{y,m} \quad (3)$$

Table 5
Average yield stress and stress at 0.003 strain.

Samples	Yield stress at 0.2% offset (MPa)	Compression strength at 0.003 strain (MPa)
Initial Al	153	184
Milled Al	592	638
Milled Al/Al_2O_3 (4 nm)	661	723

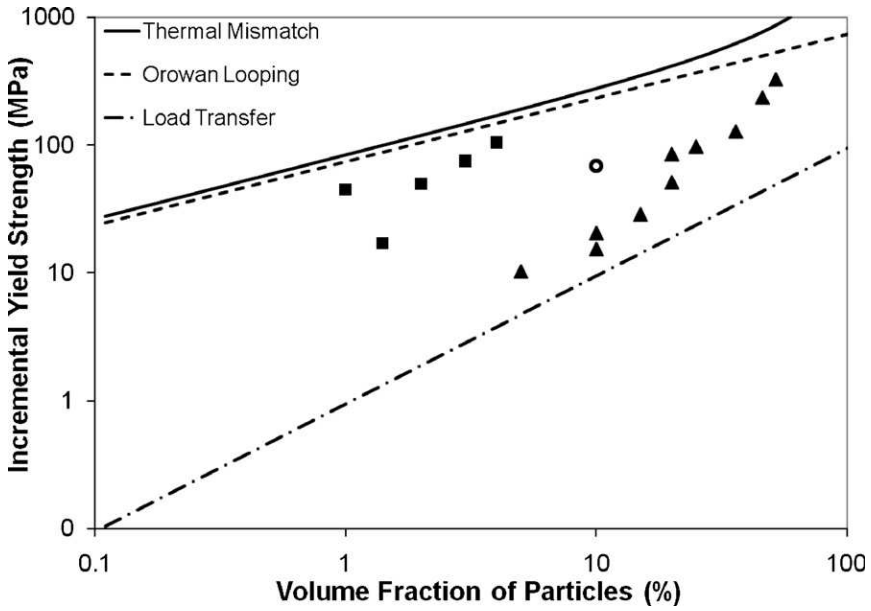

Fig. 11. Incremental yield strength with Al_2O_3 addition. The triangles and squares represent experimental results for Al_2O_3 particle size above and below 500 nm respectively [3,30,31]. The circle represents the experimental result obtained in this study.

where σ_c is the composite yield strength, V_p is the volume fraction of alumina, σ_p is the Al_2O_3 stress calculated assuming equal deformation of the matrix and the reinforcement and $\sigma_{y,m}$ is the aluminum yield strength.

Thermal mismatch was modeled using Arsenault equation [22], based on the assumption that the reinforcements are parallelepipeds where prismatic punching occurs equally on all faces. The dislocation density generation (ρ) is found to be:

$$\rho = \frac{4V_p\varepsilon_{therm}}{b(1-V_p)}\left(\frac{1}{t_1}+\frac{1}{t_2}+\frac{1}{t_3}\right) \quad (4)$$

where ε_{therm} is the thermal strain, b is the Burger's vector and t_{1-2-3} are the reinforcement height, width and thickness assuming parallelepiped particles.

The corresponding increase in strength of the composite can be calculated from [22]:

$$\Delta\sigma = \alpha G\rho^{1/2}b \quad (5)$$

where α is a constant equal to 1.25 and G is the shear modulus of the matrix. While this model was initially developed for micron size particulates, recent studies have shown that it might be one of the main strengthening mechanisms for nanocomposites [23–25].

Orowan looping model calculates the resistance of the second phase to the passage of dislocations from a balance between the force acting on the dislocation and the force coming from the line tension acting on both sides of the bulge. It has been modified by Ashby to take into account the distribution of particle spacings and the size of the particles (Ashby–Orowan equation) [26]:

$$\Delta\tau_y = 0.84\frac{1.2Gb}{2\pi\langle L\rangle}\ln\frac{\langle r\rangle}{b} \quad (6)$$

where $\Delta\tau_y$ is the increase in shear stress, $\langle L\rangle$ is the average interparticle spacing and $\langle r\rangle$ is the average particle radius. The increase in shear stress can be converted to an increase in yield strength from:

$$\Delta\sigma_y = M_T\ \Delta\tau_y \quad (7)$$

where M_T is the Taylor factor.

The average particle radius of Orowan model $\langle r\rangle$ is defined as the average particle radius measured from a polished surface, or intersection radius. This intersection radius was calculated from the particle diameter (D, 25 nm) with equation [26]:

$$\langle r\rangle = \frac{D}{\sqrt{6}} \quad (8)$$

The average interparticle spacing $\langle L\rangle$ is defined in this model as the number of particles seen in a polished surface per unit area. It was calculated from the volume fraction V_p and the intersection radius using this equation:

$$\langle L\rangle = \left(\frac{\pi D^2}{6V_p}\right)^{1/2} \quad (9)$$

While the strengthening mechanisms are evaluated separately in this study to first understand the significance of each of them, it is believed that an additive or synergetic effect probably occurs combining several mechanisms [23].

The parameters used in the various models are shown in Table 6.

The results obtained from those simulations were compared with the yield strength obtained in this study as well as experimental values from literature in Fig. 11.

The incremental yield strength values obtained from thermal mismatch and Orowan looping models are very similar and much higher than the values predicted by the load transfer model. Load shearing between the matrix and reinforcement is at the origin of the mechanical behavior of composite with high volume fraction of reinforcement with high aspect ratio, such as with continuous composites. However, in situ strengthening of the matrix will dominate for most discontinuous metal matrix composite, as it is the case here [32].

Table 6
Parameters for Al_2O_3 strengthening models.

Parameters	Value
E_p [27]	300 GPa
E_m [25]	70 GPa
$\sigma_{y,m}$ [28]	0.029 GPa
ε_{therm} [27]	0.006708
b [28]	0.286 nm
t_{1-2-3}	25 nm
G [25]	26.4 GPa
M_T [29]	3.1

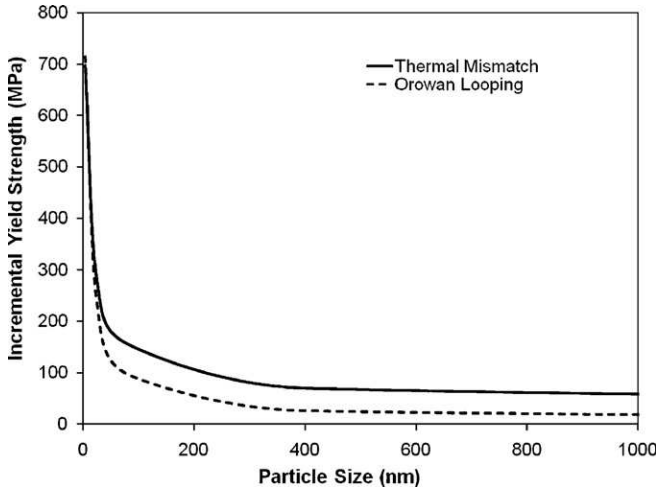

Fig. 12. Incremental yield strength of the 10 vol% Al_2O_3/Al composite modeled for various particle sizes.

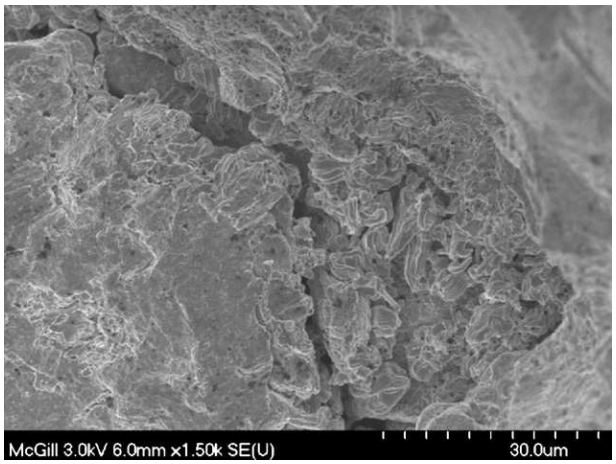

Fig. 14. Lack of bonding between particles after consolidation by hot pressing of the 10 vol% Al_2O_3 (80 nm) sample.

The incremental yield strength obtained from the Al_2O_3/Al composite produced in this study is much higher than the gain obtained from micron size Al_2O_3/Al composite with the same concentration. Fig. 12 shows the effect of particle size on the thermal mismatch and Orowan looping models. It is seen that particle size has a strong impact of the modeled yield strengths. It is stated in literature that the Orowan effect is insignificant for particle sizes above 1 μm [33]. The current simulation, with a predicted gain in yield strength due to Orowan looping of only 12 MPa for particle size of 1 μm, is in agreement with this statement. At this size, the interparticle distances are too high to impede dislocation motion. The thermal mismatch model predicts a higher gain of 44 MPa in the same condition, which is more significant. For smaller reinforcement, especially below 100 nm, the gains in yield strength predicted by the thermal mismatch and Orowan looping models increase drastically. According to the thermal mismatch model, smaller second phase will generate more dislocations because more particles are present for the same concentration. In the case of Orowan looping model, smaller second phase decreases the average interparticle spacing, and thus increases the second phase resistance to dislocation. This increase in matrix strengthening is at the origin of the higher gains in strength obtained for nanocomposites compared to composites with micron size reinforcement. Since the predictions from the two models are very similar, TEM observation of dislocations would be needed to identify the proper strengthening mechanism involved. In this study, no evidence of dislocation loops or bowing were observed in the 10 vol% Al_2O_3 thin film. However, no clear conclusion can be drawn because most high resolution observations were performed with the STEM: its convergent beam does not allow easy distinction of dislocations in the bright field mode.

By extrapolating in Fig. 11 the gains in yield strength obtained from previous studies involving nanosize Al_2O_3 addition at low concentration, one would expect higher gain than the one obtained in this study. Also, the present yield strength does not match the predicted yield strengths from the thermal mismatch and Orowan looping models. As explained for the microhardness measurements, the few nano-particle aggregates present in the compact could reduce the effective nano-particle content. Also, the lower value is probably partly due to the lack of consolidation during cold and hot pressing. Even if some clear Al interfaces are observed as seen in the BF-STEM images in Fig. 13a, significant amount of porosity remains in the compact, as observed in Fig. 13b. The compact densities, indicated in Table 4, are around 95%. The observation of the fracture surfaces of the composites has shown a lack of bonding between Al particles, as seen in Fig. 14. Also, the bonding between the Al_2O_3 and the Al matrix was limited. Fig. 15 shows ZC-STEM

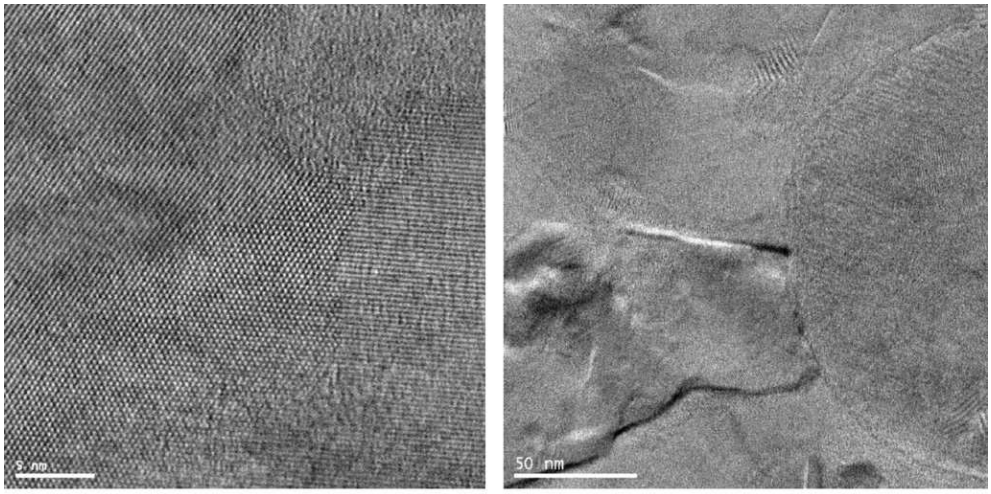

Fig. 13. BF-STEM images of (a) coherent Al interfaces and (b) void at Al interfaces, in the hot pressed 10 vol% Al_2O_3 (80 nm) sample.

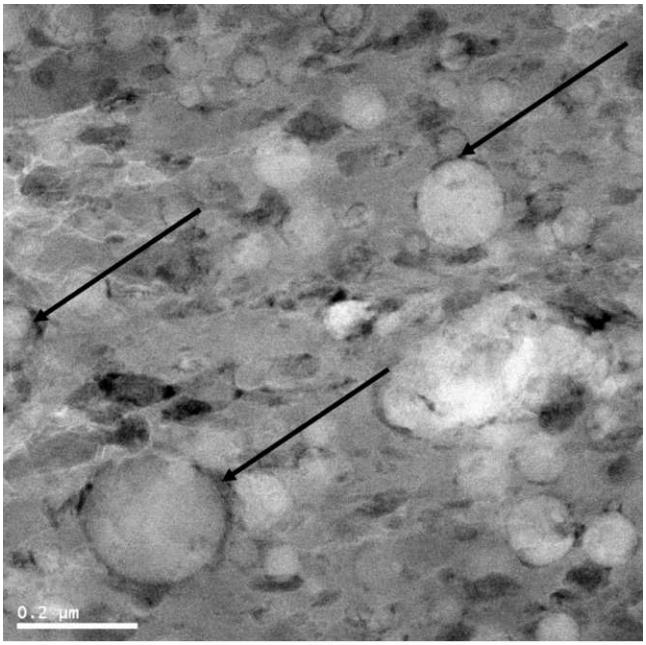

(a)

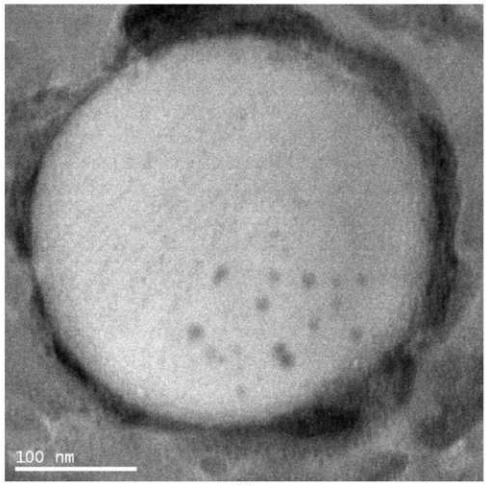

(b)

Fig. 15. (a) Low and (b) high magnification ZC-STEM pictures of the cavities at the Al_2O_3/Al interfaces after consolidation by hot pressing of the 10 vol% Al_2O_3 (80 nm).

pictures from the thin film sample prepared by FIB where a large number of cavities are visible at the Al_2O_3/Al interface. Mechanical milling reduces the compressibility of the powders due to work hardening occurring during milling [34]. Also, Al_2O_3 particles act as barriers that slow down the diffusion process required for proper sintering [35]. A secondary processing, such as extrusion, would certainly help to improve the composite densification and properties. It would also be interesting to consolidate the powder through cold spray technique. Cold spray has been used to deposit successfully nanocrystalline Al [36] as well as some nanocomposites [37]. Work is currently being done in this regard [19]. The low temperature involved in the process preserves the grain size of the powders and the hardness/strength gain associated to it [36].

It is worth mentioning that the incremental yield strength of this study was obtained by subtracting the yield strength value of the compact made from milled aluminum from the value of the compact made from aluminum milled with Al_2O_3. It is assumed that the strengthening effect of milling is independent of Al_2O_3 addition and that it can be subtracted to obtain incremental yield strength solely due to traditional strengthening effects of Al_2O_3 addition. However, the presence of Al_2O_3 modifies the milling behavior by accelerating deformation. Also, it is unknown if the strengthening effect of milling and the reinforcement traditional strengthening effects are additive.

4. Conclusions

In this paper, mechanical milling was investigated as a possible way to disperse uniformly n-Al_2O_3 in Al powder. It was found that the Al_2O_3 composites resulting from milling display a uniform dispersion of the second phase with few agglomerates of around 1 micron in size. The Al_2O_3/Al nanocomposite powders hardness is near five times higher than pure unmilled Al. A decrease in the Al_2O_3 particle size from 400 to 4 nm has increased the nanocomposite powder hardness of 11%. Presence of Al_2O_3 also affects the grain refinement occurring during milling. Compression tests performed on the hot pressed compacts have shown similar trends with a final yield stress and compression strength of 661 and 723 MPa respectively for the 10 vol% Al_2O_3 (4 nm) composite. The observed strengthening is associated to grain refinement and dispersoid formation from mechanical milling together with in situ matrix strengthening from the addition of the n-Al_2O_3. Finally, in order to counteract the lack of consolidation obtained from hot pressing of the milled powders, cold spray technique is currently investigated as a possible alternative.

Acknowledgements

This work is financially supported by the National Research Council of Canada (NSERC), “Fonds québécois de la recherche sur la nature et les technologies” (FQRNT) and Nanoquebec. The 80 nm size Al_2O_3 powder was provided by David Frost, from McGill. The authors would like to thank Dr. Xue Dong Liu, Slavek Poplawski and Ronald Sheppard from McGill University for TEM operations, XRD measurements and compression testing and René Veillette from IREQ for the FIB sample preparation.

References

[1] I. Sinclair, P.J. Gregson, Mater. Sci. Technol. 13 (1997) 709–726.
[2] D.J. Lloyd, Int. Mater. Rev. 39 (1994) 1–23.
[3] Y.-C. Kang, S.L.-I. Chan, Mater. Chem. Phys. 85 (2004) 438–443.
[4] S. Mula, P. Padhi, S.C. Panigrahi, S.K. Pabi, S. Ghosh, Mater. Res. Bull. 44 (2009) 1154–1160.
[5] Z.Y. Ma, Y.L. Li, Y. Liang, F. Zheng, J. Bi, S.C. Tjong, Mater. Sci. Eng. A 219 (1996) 229–231.
[6] S.F. Hassan, M. Gupta, Mater. Sci. Eng. A 392 (2005) 163–168.
[7] S. El-Eskandarany, J. Alloys Compd. 279 (1998) 263–271.
[8] Z.R. Hesabi, A. Simchi, S.M.S. Reihani, Mater. Sci. Eng. A 428 (2006) 159–168.
[9] J. Naser, W. Riehemann, H. Ferkel, Mater. Sci. Eng. A 234–236 (1997) 467–469.
[10] H. Ferkel, B.L. Mordike, Mater. Sci. Eng. A 298 (2001) 193–199.
[11] F. Tang, M. Hagiwara, J.M. Schoenung, Mater. Sci. Eng. A 407 (2005) 306–314.
[12] Powder obtained from David Frost, Associate professor, Department of Mechanical Engineering, McGill University.
[13] C.J. Rocha, R.M. Leal Neto, V.S. Goncalves, L.L. Carvalho, F. Ambrozio Filho, Mater. Sci. Forum 416–418 (2003) 144–149.
[14] C. Suryanarayana, M. Norton, X-Ray Diffraction: A Practical Approach, Plenum, New York, 1998.
[15] J. Langford, D. Louer, P. Scardi, J. Appl. Crystallogr. 33 (2000) 964–974.
[16] M. Kawasaki, Y. Huang, C. Xu, M. Furukawa, Z. Horita, T.G. Langdon, Mater. Sci. Eng. A 410–411 (2005) 402–407.
[17] A.S. Khan, B. Farrokh, L. Takacs, Mater. Sci. Eng. A 489 (2008) 77–84.
[18] C. Suryanarayana, Prog. Mater. Sci. 46 (2001) 1–184.
[19] D. Poirier, J.G. Legoux, R.A.L. Drew, R. Gauvin, J. Therm. Spray Technol., in press.
[20] F. Zhou, J. Lee, E.J. Lavernia, Scripta Mater. 44 (2001) 2013–2017.
[21] J. Bailon, J. Corlot, Des matériaux, Presses internationales Polytechnique, Montreal, 2000.
[22] R.J. Arsenault, N. Shi, Mater. Sci. Eng. A 81 (1986) 175–187.
[23] Z. Zhang, D.L. Chen, Scripta Mater. 54 (2006) 1321–1326.
[24] H. Liu, C. Huang, X. Teng, H. Wang, Mater. Sci. Eng. A 487 (2008) 258–263.

[25] R. George, K.T. Kashyap, R. Rahul, S. Yamdagni, Scripta Mater. 53 (2005) 1159–1163.
[26] T. Gladman, The Physical Metallurgy of Microalloyed Steels, Institute of Materials, London, 1997.
[27] Alumina and alumina fibres—properties and applications—suppliers data by Goodfellow, AZo Journal of Materials Online, edited by Azomaterials, www.azom.com/details.asp?ArticleID=2103.
[28] K.T. Kashyap, C. Ramachandra, C. Dutta, B. Chatterji, Bull. Mater. Sci. 23 (2000) 47–49.
[29] M. Song, Mater. Sci. Eng. A 443 (2007) 172–177.
[30] K.S. Raju, V.V. Bhanu Prasad, G.B. Rudrakshi, S.N. Ojha, Powder Metall. 46 (2003) 219–223.
[31] M.K. Aghajanian, R.A. Langensiepen, M.A. Rocazella, J.T. Leighton, C.A. Anderson, J. Mater. Sci. 28 (1993) 6683–6690.
[32] T.W. Clyne, P.J. Withers, An Introduction to Metal Matrix Composites, Cambridge University Press, Cambridge, 1993.
[33] W.S. Miller, F.J. Humphreys, Scripta Metall. Mater. 25 (1991) 33–38.
[34] J.B. Fogagnolo, E.M. Ruiz-Navas, M.H. Robert, J.M. Torralba, Mater. Sci. Eng. A 355 (2003) 50–55.
[35] R.M. German, Sintering Theory and Practice, Wiley, New York, 1996.
[36] L. Ajdelsztajn, B. Jodoin, G.E. Kim, J.M. Schoenung, Metall. Mater. Trans. A 36 (2005) 657–666.
[37] P. Sudharshan Phani, V. Vishnukanthan, G. Sunderarajan, Acta Mater. 55 (2007) 4741–4751.